8. Appendix

Defining the Distance of $\mathscr{H}$ from $\mathscr{H}_0$

Fenichel theory implies that $\mathscr{H}$ converges to $\mathscr{H}_0$ with decreasing ε [Fenichel, 1979]. A natural question is then how close $\mathscr{H}_0$ and $\mathscr{H}$ are to each other for $\varepsilon = 0.0037$. To investigate the distance of $\mathscr{H}$ from $\mathscr{H}_0$, we stratify the surfaces into intersections with sections $\Lambda = \{\omega \in \mathbb{R}^4 \mid \omega_B = \widehat{B}\}$ for several values of $\widehat{B}$. We denote intersections $\mathscr{H} \cap \Lambda := \mathscr{H}^{\widehat{B}}$ and $\mathscr{H}_0 \cap \Lambda := \mathscr{H}_0^{\widehat{B}}$, respectively. A $\widehat{B}$-dependent integral norm of the difference between $\mathscr{H}^{\widehat{B}}$ and $\mathscr{H}_0^{\widehat{B}}$ in Λ can then be computed to give an idea of the distance of $\mathscr{H}$ from $\mathscr{H}_0$.

Any $\mathscr{H}_0^{\widehat{B}}$ can readily be obtained by including the requirement that $B = \widehat{B}$ in the computation of $\mathscr{H}_0$. We increase the mesh size for accuracy in the computation and take $r_2 = 1 \times 10^{-3}$. Since we do not intend to render a surface after the computation of $\mathscr{H}_0^{\widehat{B}}$, it is not necessary here to keep the mesh size constant for all $\widehat{B}$.

To compute $\mathscr{H}^{\widehat{B}}$, we could use a computer package such as MATLAB to approximate the intersection curve $\mathscr{H}^{\widehat{B}} = \mathscr{H} \cap \Lambda$ from the data of the computed surface $\mathscr{H}$. However it is much more accurate and elegant to compute $\mathscr{H}^{\widehat{B}}$ via continuation, which works as follows. We first follow the steps for computing $\mathscr{H}$ and stop the continuation when $\mathbf{u}(0)_B = \widehat{B}$ instead of sweeping out the entire surface. We then replace conditions (17) and (18) with the new boundary conditions

$$\mathbf{u}(0) \in \Lambda \tag{31}$$

and

$$\mathbf{w}(0) \in \Lambda \tag{32}$$

and continue the one-parameter family of paired orbit segments $(\mathbf{w}, \mathbf{u})$ satisfying (19), (20), (21), (22), (31), and (32) with varying $\mathbf{u}(0)_A$ and T. The curve $\mathscr{H}^{\widehat{B}}$ is then given as the one-parameter family $\mathbf{u}(0)$.

The three-dimensional section Λ for fixed $\widehat{B}$ is divided into two regions by a two-dimensional surface of points at which the vector field (1) is tangent to Λ in the B-direction; this happens when $\frac{dB}{dt} = 0$, that is, when $X = 1/\widehat{B} - AY$ according to (1). This surface, called a tangency locus [Lee *et al.*, 2008], divides the curve $\mathscr{H}^{\widehat{B}}$ into two parts: along one part the flow of (1) is from left to right (from larger to smaller values of B), and along the other the flow is from right to left. Our algorithm computes both pieces of $\mathscr{H}^{\widehat{B}}$, corresponding to the pieces of $\mathscr{H}$, shown in Figure 19, in a single run; see also [**?**]. The two pieces are distinguished by the properties of the paired orbit segments $(\mathbf{w}, \mathbf{u})$ that represent orbits on $\mathscr{H}$. Each panel of Figure 19 shows one of the two pieces of $\mathscr{H}$ computed for $\widehat{B} = 0.75$ with the $\mathbf{w}$-family plotted in red and the $\mathbf{u}$-family plotted in blue. Panel (a1) shows a global view of the portion of $\mathscr{H}$ for which the flow moves from left to right through $\mathbf{u}(0) \in \mathscr{H}^{\widehat{B}}$. Panel (a2) is an enlargement of the region where $\mathscr{H}$ intersects Λ. An example orbit segment is shown in forest green and magenta, and we can see that $\mathbf{u}(0)$ lies in the spiralling region of $\mathscr{H}$. Panel (b1) shows a global view of the portion of $\mathscr{H}$ for which the flow through $\mathbf{u}(0)$ moves from right to left. Panel (b2) is an enlargement of the region where $\mathscr{H}$ intersects Λ, illustrating with an example orbit segment that $\mathbf{u}(0)$ lies in a non-spiralling region of $\mathscr{H}$. Note that the orbit segments $\mathbf{u}$ in panels (a1) and (a2) have the segments to the right of Λ in common with the orbit segments $\mathbf{w}$ in panels (b1) and (b2). The pieces of $\mathscr{H}$ shown in Figure 19(a1) and Figure 19(b1) do not constitute the entire surface $\mathscr{H}$. This is due to the strong contraction in backward time near C^2, which results in many $(\mathbf{w}, \mathbf{u})$-pairs being indistinguishable numerically in terms of the end point $\mathbf{u}(0)$.

Once computated as described above, we compare $\mathscr{H}_0^{\widehat{B}}$ and $\mathscr{H}^{\widehat{B}}$ inside Λ for several choices of $\widehat{B} \in (H_B, F_{1_B})$. Figure 20 shows intersection curves $\mathscr{H}_0^{\widehat{B}}$ (green) plotted on top of $\mathscr{H}^{\widehat{B}}$ (purple) for $\widehat{B} = 0.8$, $\widehat{B} = 0.75$, $\widehat{B} = 0.62$, and $\widehat{B} = 0.4$ (left to right) in projection onto (B, A, X)-space. Recall that the boundary of $\mathscr{H}_0^{\widehat{B}}$ is $(C^2 \cup C^3) \cap \Lambda$ and the boundary of $\mathscr{H}^{\widehat{B}}$ is $(S^2 \cup S^3) \cap \Lambda$. Therefore, differences in the boundary points of $\mathscr{H}^{\widehat{B}}$ and $\mathscr{H}_0^{\widehat{B}}$ are expected, because S^3 and S^2 lie $O(\varepsilon)$ away from C^3 and C^2, respectively. Near S^3, the boundary point of $\mathscr{H}_0^{\widehat{B}}$ has a larger A-value, and, in the spiralling region near

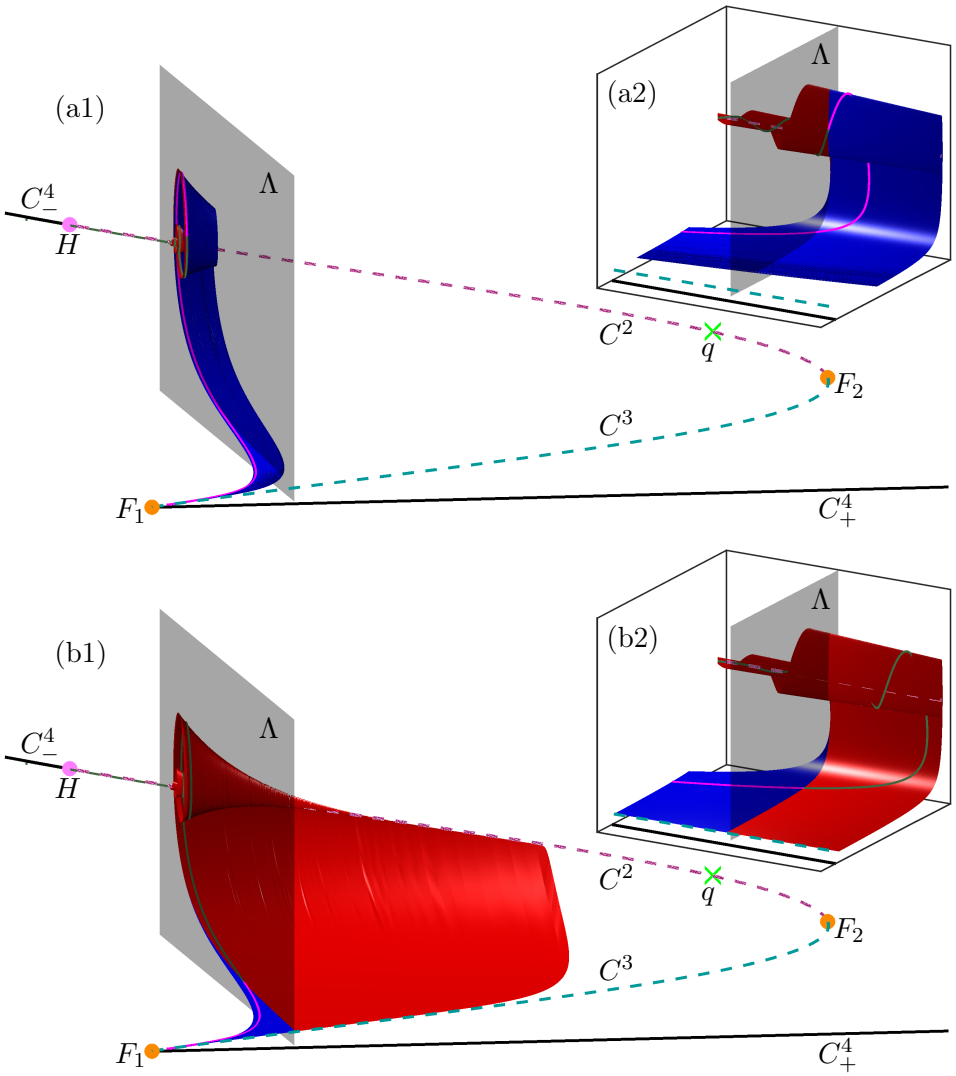

Fig. 19. Computation of the intersection curve $\mathscr{H}^{\widehat{B}}$ in Λ (charcoal surface) for $\widehat{B} = 0.75$, shown in projection onto (B, A, X)-space. Row (a) shows the pairs $(\mathbf{w}, \mathbf{u})$ used to compute the upper part of $\mathscr{H}^{\widehat{B}}$ when $\mathbf{w}$ is entirely to the left of Λ; and row (b) shows the pairs $(\mathbf{w}, \mathbf{u})$ used to compute the lower part of $\mathscr{H}^{\widehat{B}}$ when $\mathbf{u}$ is entirely to the left of Λ. Here the surface traced out by $\mathbf{w}$ is red with a sample orbit in forest-green, and the surface traced out by $\mathbf{u}$ is colored blue with a sample orbit in magenta. Panels (a1) and (b1) provide the respective global view and panels (a2) and (b2) are enlargements near Λ.

S^2, the boundary point of $\mathscr{H}_0^{\widehat{B}}$ has a smaller A-value than the boundary points of $\mathscr{H}^{\widehat{B}}$. The difference between boundary points of $\mathscr{H}^{\widehat{B}}$ and boundary points of $\mathscr{H}_0^{\widehat{B}}$ is only visible in Figure 20 for $\widehat{B} = 0.4$. There is also a noticeable difference between the respective two curves farther away from the boundary points in areas where $\mathscr{H}_0^{\widehat{B}}$ and $\mathscr{H}^{\widehat{B}}$ spiral. We can see that more spiraling corresponds to a larger distance between the curves; in other words, the difference between $\mathscr{H}^{\widehat{B}}$ and $\mathscr{H}_0^{\widehat{B}}$ is more pronounced for $\widehat{B}$ closer to H_B.

It is a difficult task to define and compute the distance between two curves in $\mathbb{R}^3$. The aproach we take here is to consider the distance of the curve $\mathscr{H}^{\widehat{B}}$ from the curve $\mathscr{H}_0^{\widehat{B}}$, by which we mean the integral of points l on the curve $\mathscr{H}_0^{\widehat{B}}$ of the distances of corresponding points in $\mathscr{H}^{\widehat{B}}$ to l. Instead the integral, we compute a corresponding sum after mesh discretization, to obtain a discretized norm. To this end, we assign a mesh of size N to $\mathscr{H}_0^{\widehat{B}}$ and index mesh points, denoted by l_i, from 1 to N, starting from those closest to C^3. This can be accomplished by fitting a spline Spl_0 to the computed data points on $\mathscr{H}_0^{\widehat{B}}$, obtained

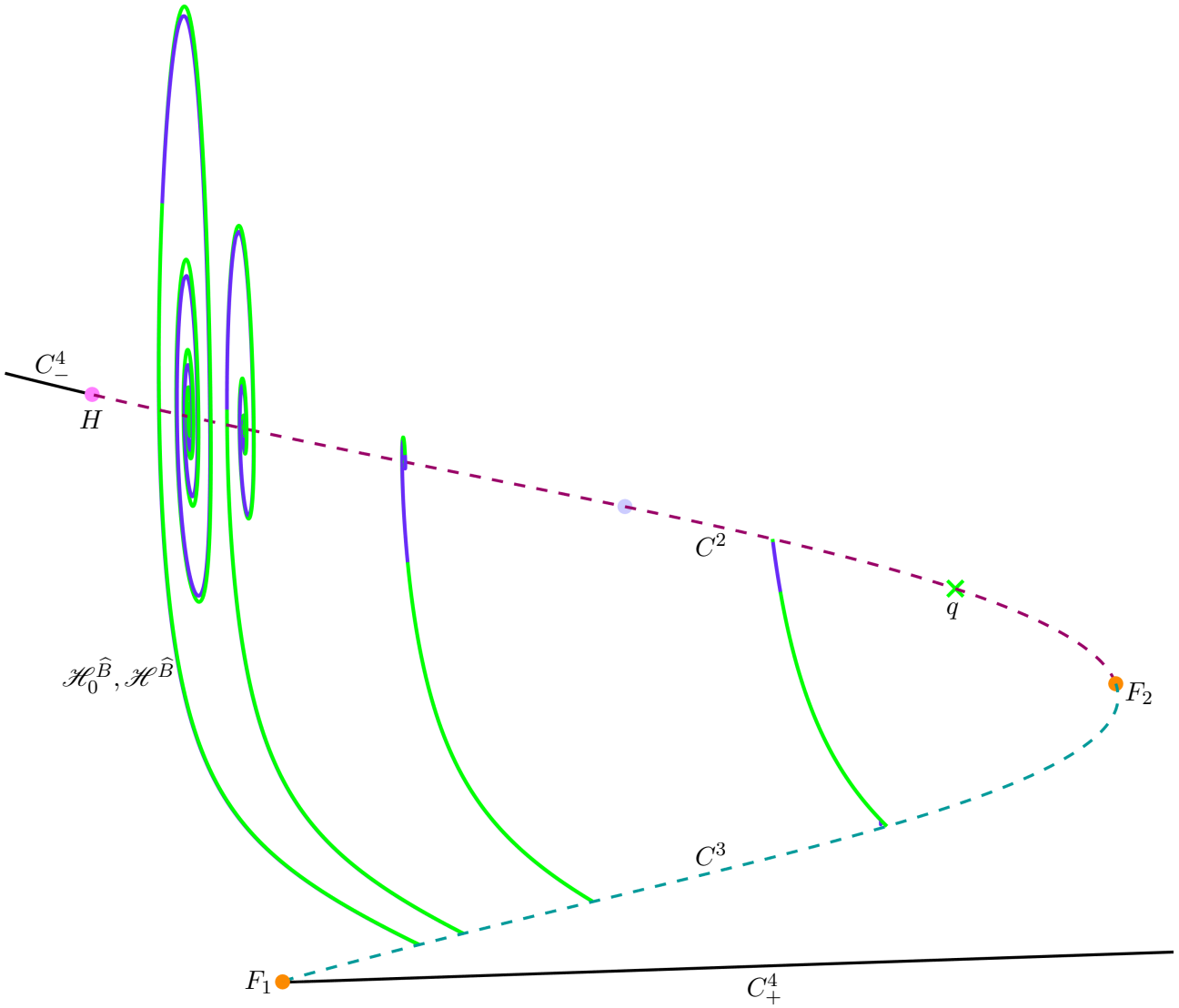

Fig. 20. Projection onto (B, A, X)-space of the intersection curves $\mathscr{H}^{\widehat{B}}$ (royal purple) of $\mathscr{H}$ and $\mathscr{H}_0^{\widehat{B}}$ (green) of $\mathscr{H}_0$ with Λ for $\widehat{B} = 0.8$, $\widehat{B} = 0.75$, $\widehat{B} = 0.62$, and $\widehat{B} = 0.4$ (left to right). The curve $\mathscr{H}^{\widehat{B}}$ is visible behind $\mathscr{H}_0^{\widehat{B}}$ only in the region where the curves are spiralling.

by continuation with AUTO. Desired mesh points can then be computed with Spl_0 at desired arclengths along $\mathscr{H}_0^{\widehat{B}}$. For each $l_i \in \mathscr{H}_0^{\widehat{B}}$, we denote the associated point on $\mathscr{H}^{\widehat{B}}$ by $k_i \in \mathscr{H}^{\widehat{B}}$. The discretized norm is then the average distance between the point pairs, given as the sum

$$d_{\widehat{B}} := \frac{1}{N} \sum_{i=1}^{N} \|l_i - k_i\| .$$

A fundamental difficulty in computing such a norm is that for every l_i, we need to make a choice of how to find k_i. This is not straightforward because there is no general way of choosing a coordinate system that defines the point k_i uniquely as a continuous function of the position of l_i. Given that $\mathscr{H}^{\widehat{B}}$ is quite close to $\mathscr{H}_0^{\widehat{B}}$, we define k_i as the closest point in the plane $\mathscr{N}_i$ through l_i that is perpendicular to (the tangent of) $\mathscr{H}_0^{\widehat{B}}$ at l_i. Hence, k_i is found as the intersection point in $\mathscr{N}_i \cap \mathscr{H}^{\widehat{B}}$ that is closest to l_i. Indeed, a fundamental issue is that in general $\mathscr{N}_i \cap \mathscr{H}^{\widehat{B}}$ may consist of more than one point, or may even be empty. This problem notwithstanding, the k_i can readily be computed for all l_i (if they exist).

Before such a computation can start, one must deal with the problem that one end of one of the two

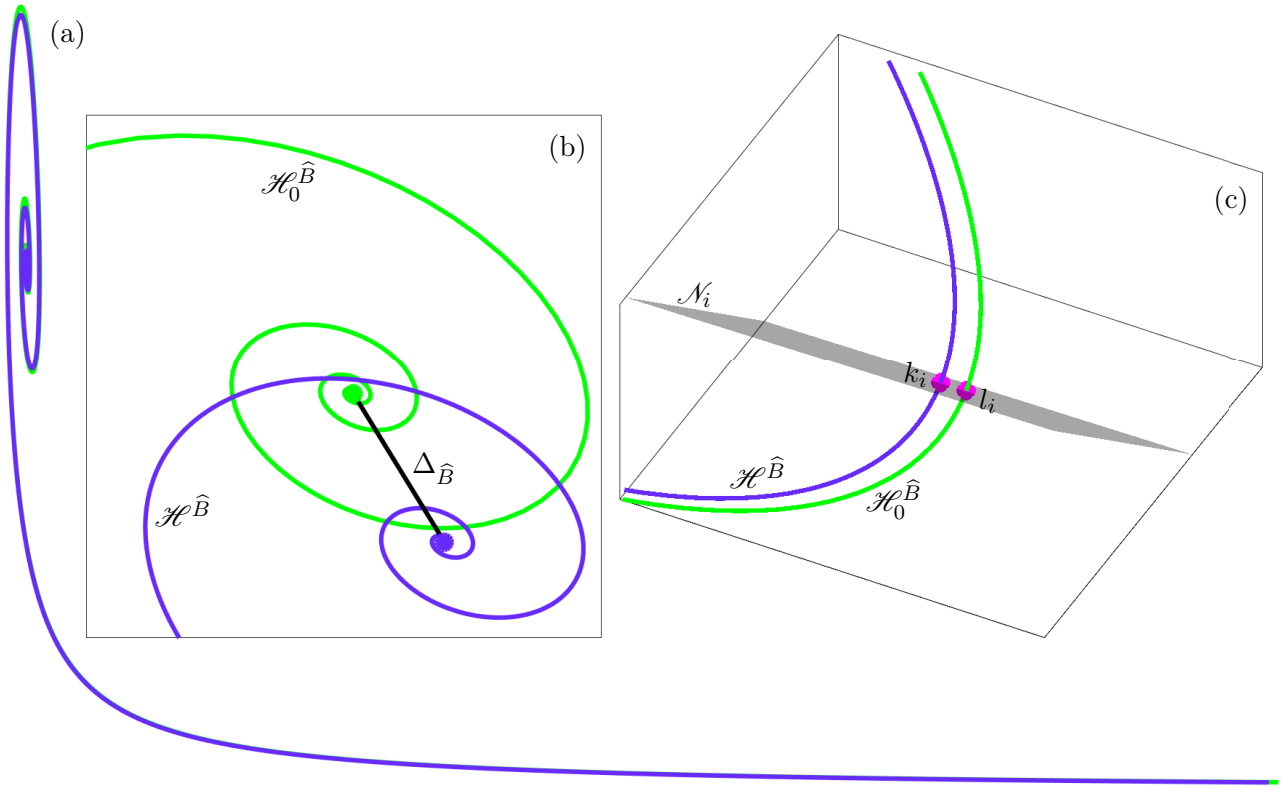

Fig. 21. Intersection curves $\mathscr{H}^{\widehat{B}}$ (royal purple) and $\mathscr{H}_0^{\widehat{B}}$ (green) for $\widehat{B} = 0.75$ projected onto the (A, X)-plane (a). An enlargement of the spiralling region near the end points of the curves is shown in panel (b) with the line of length $\Delta_{\widehat{B}}$ connecting them. Panel (c) shows a further enlargement of the spiralling region inside the section Λ, represented by (A, X, Y)-space, with the plane $\mathscr{N}_i$ (charcoal surface) that is normal to $\mathscr{H}_0^{\widehat{B}}$ at the point l_i (magenta dot). The corresponding point k_i on $\mathscr{H}^{\widehat{B}}$ is also shown in magenta.

curve 'sticks out' beyond the end point of the other curve, so that l_i near the boundary points of $\mathscr{H}_0^{\widehat{B}}$ may not have appropriate matches k_i on $\mathscr{H}^{\widehat{B}}$; see Figure 20(a), where $\mathscr{H}_0^{\widehat{B}}$ (green curve) and $\mathscr{H}^{\widehat{B}}$ (purple curve) are shown for $\widehat{B} = 0.75$. To avoid this problem, we first truncate $\mathscr{H}_0^{\widehat{B}}$ near C^3 so that at its first (mesh) point the plane normal to $\mathscr{H}_0^{\widehat{B}}$ intersects the first computed data point of $\mathscr{H}^{\widehat{B}}$. At their other end points, the two curves approach C^3 and S^3, respectively, and we denote by $\Delta_{\widehat{B}}$ the distance between these two computed end points, representing $C^3 \cap \Lambda$ and $S^3 \cap \Lambda$; see Figure 20(b), where $\Delta_{\widehat{B}} \approx 0.009796$ is represented by a connecting black line. Where the curves do not spiral we truncate $\mathscr{H}_0^{\widehat{B}}$ with a perpendicular plane as near C^3. However, where $\mathscr{H}_0^{\widehat{B}}$ spirals into C^3, this approach is not suitable; instead we truncate $\mathscr{H}_0^{\widehat{B}}$ in the spiralling region so that its last (mesh) point has distance $2\Delta_{\widehat{B}}$ from $C^3 \cap \Lambda$.

With the built in MATLAB function SPLINE, we fit splines Spl_0 and Spl to the truncated curves $\mathscr{H}_0^{\widehat{B}}$ and $\mathscr{H}^{\widehat{B}}$, respectively. Apart from the truncated end points, we choose the set of computed data points obtained from the AUTO continuation as the mesh points l_i on $\mathscr{H}_0^{\widehat{B}}$, which gives a mesh with well over $N = 700$ mesh points. For each l_i, we apply the built-in MATLAB function FNDER to Spl_0 to obtain a unit tangent vector, which is then used to define $\mathscr{N}_i$. The points $k_i \in \mathscr{N}_i$ are then computed with the spline function Spl. The enlargement in Figure 21(c) shows a representative (l_i, k_i)-pair (magenta dots) on $\mathscr{H}_0^{\widehat{B}}$ and $\mathscr{H}^{\widehat{B}}$, respectively, and the corresponding $\mathscr{N}_i$ (charcoal plane). This is the situation, like for most points l_i, where there is (locally) a unique intersection point. Indeed, there are generally other intersection points with $\mathscr{N}_i$ much further away when $\mathscr{H}_0^{\widehat{B}}$ and $\mathscr{H}^{\widehat{B}}$ are spiralling, and this if why we choose k_i to be the intersection with the smallest arclength distance from k_{i-1}, which is locally consistent.